Journal Name

Dynamic Article Links ►

Cite this: DOI: 10.1039/c0xx00000x

www.rsc.org/xxxxxx

ARTICLE TYPE

Carbene Iridium Complexes for Efficient Water Oxidation: Scope and Mechanistic Insights

James A. Woods,[a] Ralte Lalrempuia,[b] Ana Petronilho,[b] Neal D. McDaniel,[a] Helge Müller-Bunz,[b] Martin Albrecht,*[b] Stefan Bernhard*[a]

Received (in XXX, XXX) Xth XXXXXXXXX 20XX, Accepted Xth XXXXXXXXX 20XX

DOI: 10.1039/b000000x

Iridium complexes of Cp* and mesoionic carbene ligands were synthesized and evaluated as potential water oxidation catalysts using cerium ammonium nitrate as a chemical oxidant. Performance was evaluated by turnover frequency at 50% conversion and by absolute turnover number, and the most promising precatalysts were subjected to further study. Molecular turnover frequencies varied from 190 to 451 per hour with a maximum turnover number of 38,000. While the rate of oxygen evolution depends linearly on iridium concentration, concurrent spectroscopic and manometric monitoring of stoichiometric additions of oxidant suggests oxygen evolution occurs as two sequential first order reactions. Under the conditions herein, the oxygen evolving species appears to be well defined and molecular based on the kinetic effects of careful ligand design, reproducibility, and the absence of persistent dynamic light scattering signals. Outside of these conditions, the complex mechanism is highly dependent on reaction conditions. While confident characterization of the catalytically active species is difficult, especially under high-turnover conditions, this work indicates IrOx is not essential for the formation of catalytically active water oxidation species.

Introduction

Global demand for energy is projected to increase significantly over the next three decades.[1] Fortunately, estimates for annual total solar insolation exceed the current and projected global demand for energy by almost four orders of magnitude.[2] Harnessing this under-utilized resource is then a natural consideration for energy researchers. Because sunlight is transient, a critical issue is the effective and efficient transformation of sunlight into a storable source of energy.[3] Despite significant improvements from multi-junction photovoltaic systems, silicon photovoltaic systems require expensive and slow-charging batteries for energy storage. Thermochemical heat engines[4] and biological mimicry[5] are also exceptionally promising technologies but rely on mechanisms resistant to controlled tuning.

A photocatalytic cycle could conceivably be tailored to function with any number of well-studied reductive pathways including carbon dioxide to methanol,[6] metal salt to metal,[7] and water to hydrogen.[8] Despite the various potential reductive pathways, complementary oxidative half-reactions producing molecular oxygen are necessary. This simplifies reactant delivery in an energy system by employing the atmosphere as an oxidant reservoir and conveyance. Water, due to its abundance and benignity, represents an ideal feedstock for this process. Unfortunately, water redox is plagued by the mechanistic complexity and high thermodynamic potential necessary to advance the oxidation reaction. Well-defined molecular catalysts are one avenue of study yielding direct characterization, structural tunability, and greater atom economy through homogenous reaction conditions.

Citing just a small portion of the broad interest in molecular water oxidation: ruthenium dimers[9–12] and tetramers,[13–15] cobalt tetramers,[16,17] manganese dimers[18] along with recent work detailing single-site catalysts[19–26] all illustrate the diversity of successful catalysts. More recently, a variety of Cp*Ir complexes (Cp* = $C_5Me_5^-$) have been shown to act as efficient water oxidation precatalysts.[27–33] These complexes are remarkable for their high activity compared to original iridium catalysts with 2-phenylpyridine ligand spheres. Mechanistic work under different reaction conditions led to controversial conclusions: while a heterogeneous mode of action has been put forward in some studies,[33–35] support for homogeneous catalysis has been obtained *e.g.* from experiments using a quartz microbalance as a probe and from catalyst immobilization.[35–37] Direct comparison of results across the broad range of mechanistic investigations reported in literature is difficult due to varying reaction conditions including the use or absence of organic co-solvents and buffered or unbuffered aqueous conditions. Following our initial discovery of triazolylidene iridium complexes as potent water oxidation catalysts, we engaged in careful ligand modification in an attempt to improve catalyst performance and to expand our understanding of oxidation mechanisms with application to a broad variety of

[a] *School of Chemistry & Chemical Biology, University College Dublin, Belfield, Dublin 4, Ireland ; E-mail: martin.albrecht@ucd.ie*

[b] *Department of Chemistry, Carnegie Mellon University, Pittsburgh, Pennsylvania 15213, United States; E-mail: bern@cmu.edu*

† Electronic Supplementary Information (ESI) available: Details on UV-vis monitoring of stepwise addition of CAN to **4a**, NMR, DLS data, and ORTEP plots of complexes **3** and **6b**, crystallographic details and cifs for the structures of complexes **1**, **3**, **4a**, **5**, **6a**, **6b**, **7**, **8**, and **11**. See DOI: 10.1039/b000000x/

fuel producing photosystems.[38–41] Here we report on the synthesis and catalytic activity in water oxidation of an expanded family of cationic Cp*Ir complexes containing either *C,C*-bidentate or a *C,N*-bidentate coordinating carbene iridium complexes.

Results and Discussion

Synthesis and characterization of the complexes

A series of cationic Cp*Ir complexes **1–10** containing either *C,C*-bidentate or a *C,N*-bidentate coordinating chelate was prepared using C–H bond activation chemistry mediated by silver cations (Scheme 1). The type of chelating sites varies considerably from the original C,C bidentate set explored previously.[28] Thus, one set of complexes features chelating *C,N*-bidentate ligands that contain a neutral *N*-bound triazole unit paired with a formally neutral abnormal pyridylidene[42] fragment (C_{pyr}, N_{trz}-bidentate; complexes **1** and **3**) or with an anionic phenyl chelate (C_{aryl},N_{trz}-bidentate; complex **2**). A second set of ligands comprises a triazolylidene core[43,44] with different substitution patterns and an *N*-bound pyridine as chelating group (N_{pyr},C_{trz}-bidentate; complexes **4–6**). *C,C*-Bidentate chelates constitute a further class of ligands, featuring a triazolylidene ligand and an anionic phenyl ligand (C_{aryl},C_{trz}-bidentate; complex **7**), or a triazolylidene and a formally neutral pyridylidene ligand (C_{pyr},C_{trz}-bidentate; complexes **8** and **9**), or an sp^3-hybridized ylidic ligand (C_{ylide},C_{trz}-bidentate; complex **10**).

The formation of complexes **1–10** provided some interesting insights into the donor properties of the ligand and the reactivity of the iridium center. In the absence of a chelating nitrogen donor, cyclometalation via C_{aryl}–H bond cleavage took place (*cf* complexes **2**, **7**). Cyclometalation involved exclusively the aryl ring bound to a nitrogen of the heterocyclic core. This reactivity pattern was observed previously also in triazolylidene palladium chemistry[45,46] and suggests an electrophilic bond activation.[47] Obviously, C_{aryl}–H activation is competitive to $C_{pyridinium}$–H bond activation, and the course of the reaction is dependent on whether N2[48] or N3 of the triazole ring is coordinated to the iridium center (*cf.* formation of a mixture of **1** and **2** from the same ligand precursor). Exchange of the aryl substituent at N1 of the ligand precursor by a methyl group prevents the formation of a chelate via N2 bonding. Consequently, exclusive coordination via N3 and ensuing $C_{pyridinium}$–H bond activation was observed, which afforded the chelating pyridylidene-triazole complex **3**.

All complexes featuring a nitrogen donor ligand were prepared in CH_2Cl_2 and were obtained as monocationic species comprising an iridium-bound chloride ligand. This chloride was readily abstracted by classical methods using AgOTf to yield the dicationic complexes. In contrast, complexes with a *C,C*-bidentate ligand were synthesized in MeCN and were isolated as the dicationic complexes directly from the iridation reaction. This behavior is in line with considerably stronger donor properties of these *C,C*-bidentate ligands compared to their *C,N*-homologues, thus inducing a higher electron density at iridium[49–51] and a destabilization of the putative Ir–Cl bond. The stronger donor properties of such abnormal formally neutral carbene ligands as compared to imines may be rationalized by their pronounced mesoionic character.[52–55] This notion enhances the relevance of a formally anionic carbon bound to the iridium center and a (remote) intermolecular stabilization of the negative charge by an iminium fragment.

Formation of complexes **4–6** with pyridine-functionalized triazolylidenes was straightforward when using equimolar ratios of iridium precursor and triazolium salt. In the presence of (slight) excess of triazolium salts, a second product appeared that was identified as the bis(carbene) complex **11** on the base of the two sets of ligand signals in the ^{1}H NMR spectrum in 1:1 ratio. The different shielding of the two sets of pyridyl protons indicates a biscarbene complex **11** comprised of one monodentate, and one *C,N*-bidentate triazolylidene ligand (Scheme 2).[56] Unambiguous confirmation of the formation of complex **11** was obtained from an X-ray diffraction analysis from crystals that grew from a reaction mixture.

The site of metalation in the new complexes **1–8** was readily deduced from NMR spectroscopic analysis of the complexes in CD_3CN solution. N-bound triazole ligands featured a diagnostic low-field signal in the 8.6–9.3 ppm range in the ^{1}H NMR

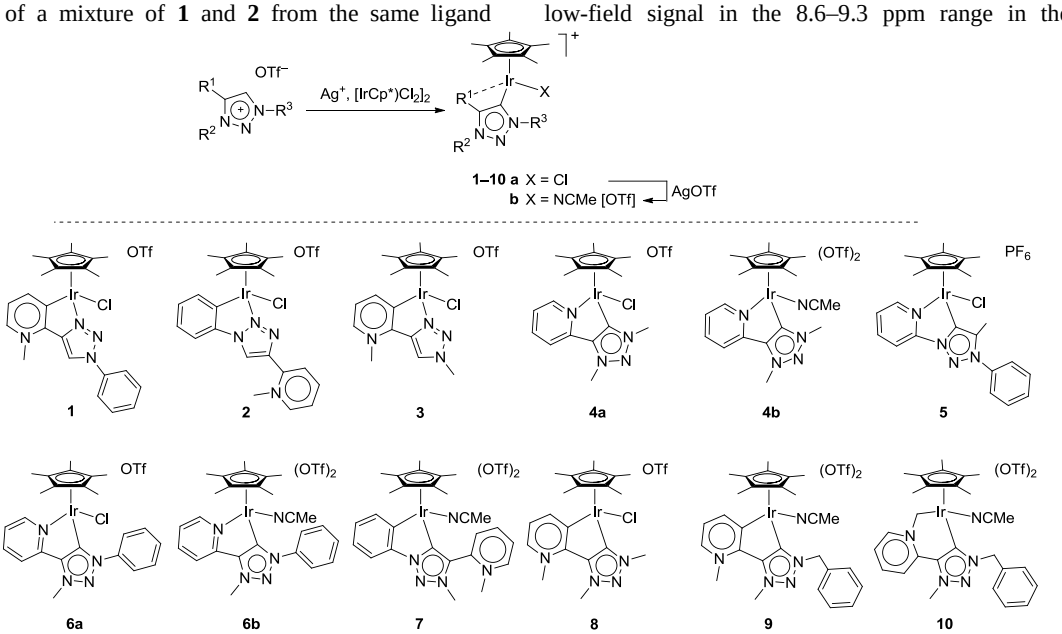

Scheme 1

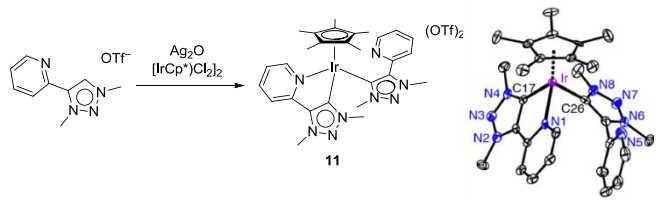

Scheme 2

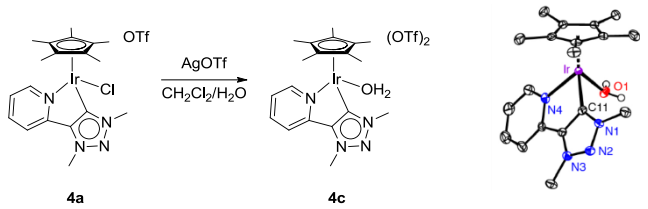

Scheme 3

spectrum due to the presence of the triazole proton at C(5) (complexes **1–3**). Pyridyline-type bonding due to $C_{pyridinium}$–H bond activation was identified by three characteristic resonances at low field (doublets at δ_H 8.7 and 8.3, and doublet of doublets at δ_H 7.6) assigned to the H(4), H(6), H(5) protons respectively of the pyridine heterocycle (complexes **1**, **3**, and **8**). In contrast, four pyridine resonances were clearly distinguishable in complexes featuring N-coordinated pyridine or non-bound pyridinium substituents (complexes **4–7**). In the ^{13}C NMR spectrum, the iridium-bound carbon of the triazolylidene ligand experiences the largest shift-difference upon metalation (δ_C around 155 in complexes **4–8**, ca. $\Delta\delta$ ca. 30 ppm compared to the ligand precursor). The pyridylidene carbon attached to iridium was observed at slightly lower field (around 160, complexes **1, 3, 8**), while the iridium-bound carbon of the phenyl group in complexes **2** and **7** appeared at 148.8 and 144.1 ppm, respectively.

In aqueous solutions, the complexes exist as equilibria between two species. The behavior of complex **4a** is representative. Two sets of pyridyl signals were observed in D_2O, the major one featuring a low field doublet for the pyridyl H(6) proton at 8.98 ppm. All signals of the minor species are downfield shifted by 0.1–0.2 ppm (*e.g.* pyridyl H(6) proton at (δ_H 9.16). The ratio of the two species is concentration and pH dependent and shifts towards the major species at high concentrations (*e.g.* 9:1 at 20 mM solution *vs.* 7:3 at 1.7 mM), indicating an equilibrium between complex **4a** and a dicationic aquo complex. In agreement with such a notion, addition of KCl completely suppresses the presence of the minor species. Likewise, in less coordinating solvents such as CD_3OD or acetone-d_6, only one species was detected. Unambiguous evidence for the formation of such a dicationic species was obtained from irreversible abstraction of the chloride in **4a** with AgOTf in aqueous CH_2Cl_2 (Scheme 3). The NMR spectrum of the formed bis(aquo) complex **4c** matches those of the minor species. Of note in particular with regards to catalytic applications is the inertness of the complexes under strongly acidic conditions. For example, spectroscopic monitoring of the stability of complex **4a** in 1 M HCl (D_2O, pH = 0) did not indicate any changes over time (> 48 h) and no diagnostic signals due to presence of triazolium or pyridinium salts were observed. Accordingly, acidolysis of the Ir–C_{trz} bond and ensuing ligand dissociation does not occur in detectable quantities under highly acidic conditions. A similar robustness was observed for the Ir–C_{pyr} bond in complex **8**, indicating that both abnormal carbene–iridium bonds are fully acid-resistant.

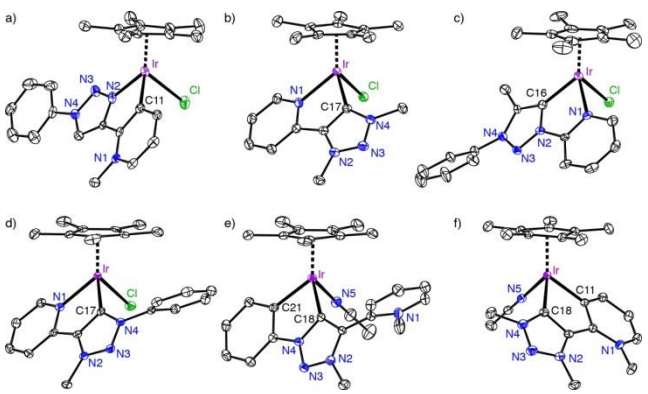

Figure 1: ORTEP representations of complexes **1** (a), **4a** (b), **5** (c), **6a** (d), **7** (e), and **8** (f); all structures at 50% probability level, hydrogen atoms, non-coordinating anions, solvent molecules, and the second independent molecule in the unit cell of **5** and **7** omitted for clarity. ORTEP plots of **3** and **6b** are shown in the supporting information (Fig. S1).

All complexes except **2** and **4b** were analyzed by single crystal X-ray diffraction. The molecular structures (Figure 1) confirmed the expected connectivity patterns. The Ir–C_{trz} bond lengths are in the expected range,[57] and are consistently shorter than the corresponding Ir–N_{trz} bond lengths. Similarly, the Ir–C_{pyr} bonds are substantially shorter than the dative Ir–N_{pyr} contacts. They are even slightly shorter than the Ir–C_{aryl} bond in complex **7**. The ligand bite angle shows little variation, as may be expected when considering that all metalacycles in complexes **1–8** are comprised of four sp^2-hybridized carbon/nitrogen atoms and that the C–N *vs* C–C bond length difference is only minute.

Table 1. Selected bond lengths (Å) and angles (in degrees) for the crystallographically analyzed complexes.

Complex (E_{trz}/E)	Ir–E_{trz}	Ir–E	E–Ir–E_{trz}
1 (N_{trz}/C_{pyr})	2.042(2)	2.053(3)	76.82(11)
3 (N_{trz}/C_{pyr})	2.068(2)	2.040(3)	77.23(9)
4a (C_{trz}/N_{pyr})	2.017(2)	2.129(2)	76.08(8)
5 (C_{trz}/N_{pyr})	2.027(6)	2.124(5)	77.5(2)
6a (C_{trz}/N_{pyr})	2.013(2)	2.134(2)	76.10(9)
6b (C_{trz}/N_{pyr})	2.032(2)	2.131(2)	76.58(9)
7 (C_{trz}/C_{aryl})	2.039(3)	2.070(3)	78.44(12)
8 (C_{trz}/C_{pyr})	2.0175(14)	2.0488(14)	76.02(6)

Catalytic activity

The reaction of complexes **3–10** with cerium(IV) ammonium nitrate was monitored with differential digital manometry as previously described and reaction end-points were verified with mass spectrometry. Stoichiometric oxygen yields (100±4%) were observed for all new complexes (Figure 2) and in contrast to previously explored catalysts,[20] no carbon dioxide was observed during later-stages of the reaction. Close inspection of the performance of **3-10** reveals distinct differences in the catalytic activity. These differences, in conjuction with persistant NMR spectra at similar pH values and ionic strength albeit in the absence of cerium, suggest retention of the carbene-containing ligands. Further evidence of ligand retention is afforded by predictable steric and electronic effects on catalyst activity however the presence of an induction period necessitates comparison of turnover frequencies at 50% conversion (Table 2).

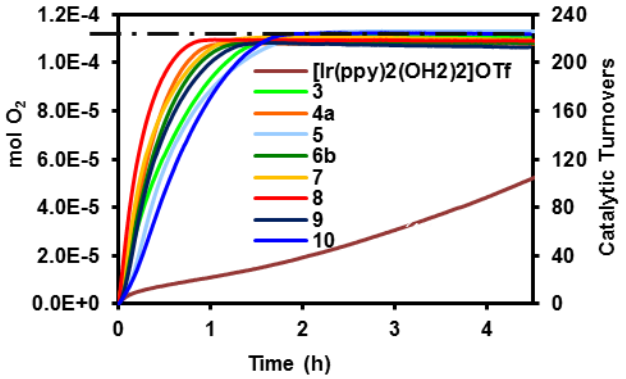

Figure 2: Catalytic activity of complexes **3–10** and $[Ir(ppy)_2(OH_2)_2]OTf$ at 0.5±0.05 mM catalyst and 0.45 M cerium(IV). Dotted line corresponds to complete stoichiometric consumption of cerium(IV).

Analogous to similar ruthenium-catalyzed water oxidation reactions,[24] steric bulk on the triazole N1 position leads to a decrease in catalytic activity (*cf* activity of **4a** *vs* **6a** and **8** *vs* **9**). Changing the ylide-carbene motif in complex **10** to a dicarbene system improved catalytic activity from 191 h^{-1} to 451 h^{-1}, suggesting the role of electronic tunability of catalytic performance. The *C*-*C* chelate appears to effect greater activity than a *N*-*C* chelate from a comparison of complexes **4a** and **8**. And, as illustrated by the poor performance of complex **3**, increasing the ligand donor properties from triazole *N*-coordination to triazolylidene *C*-bonding (c.f. **8**) is beneficial and leads to greater activity.

Table 2. Turnover frequencies at 50% conversion, TOF_{50}

Complex	**3**	**4a**	**5**	**6a**	**7**	**8**	**9**	**10**
TOF_{50} (h^{-1})	190	365	197	301	327	451	279	191

In contrast to reports suggesting the formation of a heterogeneous species implicated as an active intermediate in the water oxidation reaction,[] exploratory reactions yielded no particles visible to the naked eye and prompted further study. While later experiments employing dynamic light scattering were able to observe the nucleation of dioxygen, no scattering attributable to iridium nanoparticles was observed from any reaction of complexes **4a**/**4c** or **8** at least to the limits of detection (ca. 0.3 nm).

Mechanistic details

Definitively interpreting the reaction progress into discrete mechanistic steps is complicated by numerous factors: the initial preequilibrium due to solvolysis, disproportionation between catalytic intermediates and various cerium(III)/cerium(IV) species[58–60], the effects of ionic strength, and the potential interactions of any supporting ions with reaction intermediates. There is also a high likelihood that reactions driven by the ostensibly single-electron oxidant cerium would have significantly different electron transfer mechanisms than periodate driven reactions which would be different still from electrode driven reactions[61–63] and render direct mechanistic comparisons inconclusive. Moreover, any investigation involving ex situ analysis, for example electron microscopy following

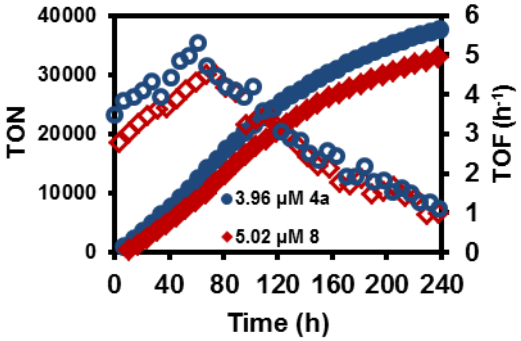

Figure 3: Turnover number and frequencies after addition of a sufficient quantity of compounds **4a** and **8** to produce the indicated concentration in 20 mL solutions of cerium ammonium nitrate (0.835M).

solvent evaporation, may lead to potentially misleading conclusions as the sample preparation will inherently affect the constitution of the observed species. We therefore set out to analyze reactions with non-invasive "*in operando*" techniques.[64]

Despite the complex reaction kinetics, important information can be garnered from in-depth investigations conducted on the most active complexes, **4a** and **8**. Turnover number and frequencies from a 5 µM solution of **8** and a 4 µM solution of **4a**, both in the presence of a saturated aqueous solution of cerium ammonium nitrate (0.835 M), are presented in Figure 3. Following an induction period, total turnovers in excess of 30,000 were common in extended oxidation experiments with 10-day turnover counts of 33,100 and 38,000 for complexes **8** and **4a** respectively.

Varying the concentration of **4a** from 1 µM to 10 µM with a strong excess of cerium(IV) further illustrates the complicated kinetics. The rate determining step appears to vary based on the concentration of **4a**, rendering a trivially interpreted rate law for the overall process difficult (Figure 4). At low catalyst

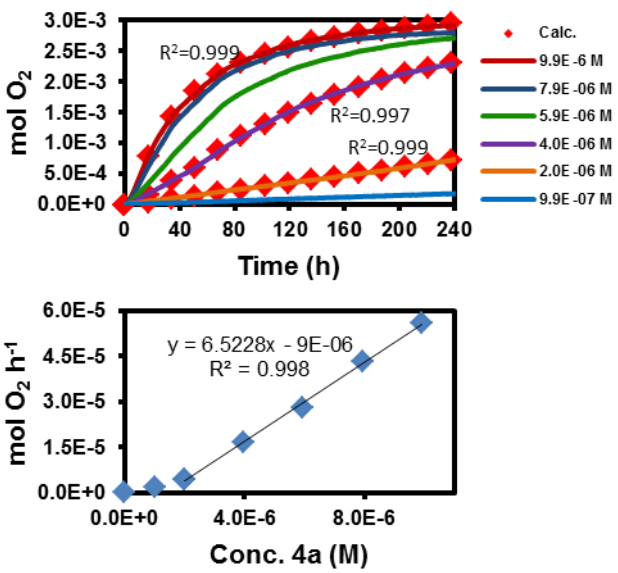

Figure 4 Top: O_2 formation for complex **4a** at concentrations ranging up to 10 µM following addition to 20 mL aqueous cerium ammonium nitrate solutions (0.835 M). The dotted trace describes a least squares fit employing the integrated rate law described in the Supporting Information. **Bottom**: Plot of maximum rate of O_2 formation from above illustrating concentration-dependent mechanism.

concentrations (≤ 2 μM), oxygen evolution was found to be linear with respect to time while at higher concentrations of **4a** (> 2 μM) the reaction appears to be limited by sequential (pseudo)first order reactions. Combined first and second-order linearized plots of the oxygen evolution traces clearly describe the two different behaviors where initial activity emulates an overall second-order reaction that gives way to slower, first-order behavior as the reaction progresses (See Figure S[illegible] a representative example as applied to the data from Figure 6). This behavior indicates the oxygen-evolving step is predicated by two sequential first order reactions (Scheme 4). As seen by the dotted traces in Figure 4, there is excellent agreement between the integrated rate law from Scheme 4 and the experimentally observed oxygen evolution data from all three regions of catalytic activity (overall second order, sigmoidal, overall first order).

Scheme 4

$$A \xrightarrow{k_{AK}} K \xrightarrow{k_{KP}} P$$

$$C_p = C_A^{\circ}\left(1 - \frac{k_{KP}\exp(-k_{AK}t) - k_{AK}\exp(-k_{KP}t)}{k_{KP} - k_{AK}}\right)$$

Additionally, the maximum rate of oxygen evolution for **4a** was found to be linearly correlated to catalyst concentration over the range of 2 μM to 10 μM with deviation from linearity at concentrations below 2 μM (Figure 4, bottom) while a log-log plot of rate vs. catalyst concentration indicates the presence of a mixed order reaction (Slope of 1.5; Supporting Information).

The effect of varying the cerium concentration from 3 mM to 0.865 M while holding the concentration of **4a** at 8.6 μM is shown in Figure 5. Cerium solutions were buffered in 1N HNO_3 for four primary reasons: to prevent the thermodynamic decay of cerium(IV) at high pH values; to avoid reaction complexity by limiting the speciation of ions present; and to take advantage of faster reaction kinetics,[65] and to preclude the precipitation of cerium(III) species. These conditions may also increase the solubility or decrease the propensity for aggregation of iridium species.

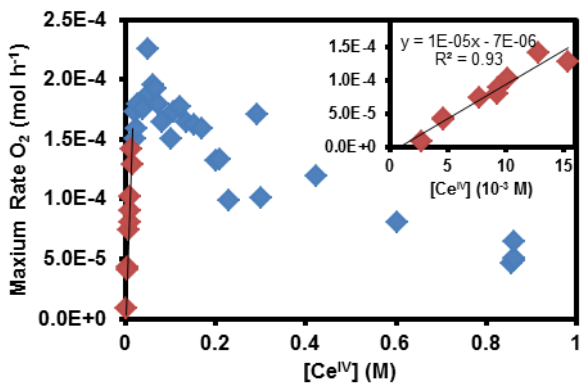

Figure 5: Variation of maximum O_2 rate due to changing cerium(IV) concentration at 8.6 μM **4a** in 1N HNO_3. Inset: Expanded scale of 0 mM to 15 mM illustrating linear trend in maximum rate at low cerium(IV) concentrations.

Under these conditions the maximum rate of oxygen production occurs at 50 mM cerium(IV) with 0.18 mmol O_2 h^{-1} (TOF 20.9 h^{-1}). Prior to this maximum, between 0-20mM cerium(IV) or roughly 300-2400 cerium(IV) equivalents, the rate of maximum oxygen evolution appears to increase linearly. A gradual decrease in the maximum rate of oxygen evolution is observed from 100 mM cerium(IV) upward. As cerium(IV) in 2M perchloric acid is believed to exist predominantly as a dimeric species,[60] this concentration-dependent inhibition could arise due to similar speciation in nitric acid or through complex equilibria as is the case with cerium(III).[66] Regardless of the actual oxidant speciation, quantitative consumption occurs in all cases over time frames greater than 10 days.

We attempted to further investigate the short-term activity under conditions where cerium is not in gross excess but quantitative consumption also occurs; this effectively probes the initial rate determining steps. As observed previously with related Ir(Cp*) complexes,[67] addition of CAN induced a color change of the initial yellow solution to blue within seconds. While the formation of a blue mixture or a blue layer[67] has periodically been attributed to IrO_x formation due to the oxide's general tendency to absorb broadly around 580 nm[30,33] similar color changes have previously been noted in high-valent iridium aquo complexes.[68] To further investigate this issue with complex **4a,** an experiment was performed using the previously described digital pressure transducers to manometrically follow the evolution of oxygen from several equal additions of oxidant with concurrent UV/Vis measurements

When a single addition of 20 equivalents of CAN was added to a 0.5 mM solution of **4a** no measurable oxygen production was observed (Figure 6) though there is a rapid color change from yellow to blue and back over the course of 15 minutes (Figure 7, Top). After 8 hours, a second aliquot of 20 equivalents of CAN was added and 8 hours later another addition of 20 equivalents. This process was repeated for a total of 8 steps or 160 total equivalents of CAN over 64 hours. A sub-stoichiometric quantity of oxygen was produced during the second through fourth additions with the deviation from stoichiometric predictions decreasing on each subsequent addition. Approximately 30 equivalents of cerium in total are unaccounted for by manometry.

No carbon dioxide was observed via headspace mass

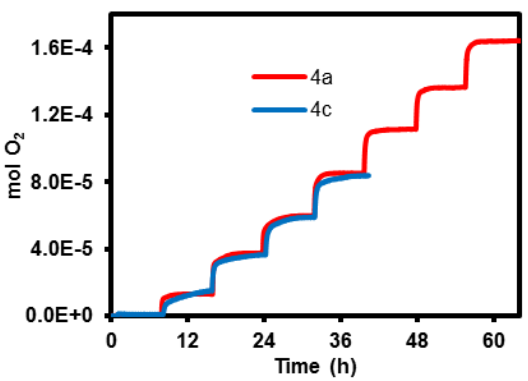

Figure 6: Stepped oxygen production following addition of 20 equivalents cerium(IV) to 0.5 mM **4a** in 1N HNO_3 with an 8 hour interval between additions overlaid with the same experiment with **4c**. No oxygen production occurs for the first thirty equivalents of cerium(IV) with stoichiometric oxygen production occurring after the third addition.

spectrometry even when the experiment was repeated with double the concentration of catalyst. The gas analyser employed is ostensibly sensitive into the ppm range; but, more conservatively if even one mole of CO_2 was produced per mole of catalyst it would occupy 1-2%mol of the overall headspace i.e. well within the limits of detection. One feasible contribution to the cerium discrepancy investigated was oxidation of the initial chloride ligand to perchlorate either by cerium or oxidized catalyst via $ClO_4^- + 4\ H_2O + 8e^- \rightarrow Cl^- + 8OH^-$ at 0.56 V. As a control, the experiment was repeated with an aquo complex, **4c**, yielding no significant differences from the chloride analogue **4a** (Figure 6, red overlay). The initial oxidant discrepancy is currently unresolved but may involve reversible cerium or peroxide speciation. Further experiments employing concurrent Raman spectroscopy are underway to determine the speciation resulting in the initial oxidant discrepancy.

Progressively examining each oxygen evolution through the method of first and second-order linearizations yields the same sequential first order behavior observed from Figure 4 however concurrent UV-vis monitoring was unable to identify clearly correlated changes in absorbance. As such, the intermediate speciation of the rate determining steps is unknown at this time. Least squares fitting of the integrated rate equation (Scheme 4) to the final four oxygen evolution steps yields first order rate constants, k_{AK} and k_{KP}, of ca. 40 hr^{-1} and 13 hr^{-1} respectively (See Supporting Information for plots and residuals). The first four steps were also evaluated but were poorly fit by the sequential first order model. The presence of an additional, faster gas-producing reaction is suggested by the initial phase of the linearization of steps 2-4.

Long-term catalyst deactivation was assessed by plotting the rate of oxygen evolution vs. the quantity of oxygen evolved[69] for the final four steps. These plots yielded overlapping traces demonstrating the absence of catalyst deactivation following the initial induction period; the active catalyst species in the experiments with a gross excess of cerium are therefore likely the same species present after the fourth addition of cerium in the stepwise experiments.

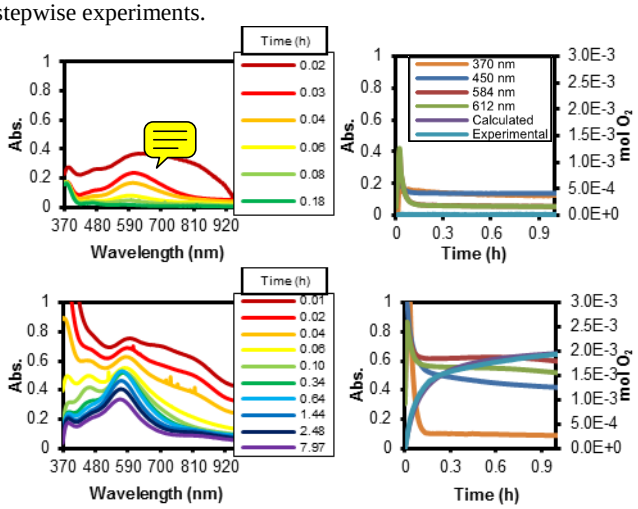

Figure 7 Left: Chronological spectra from the first (top) and fourth (bottom) addition of 20 equivalents cerium(IV). Spectra are indexed in hours relative to the preceding cerium(IV) addition. **Right**: Absorbance traces with experimental and calculated oxygen evolution traces in purple and light blue for the first (top) and fourth (bottom) addition of 20 equivalents of cerium(IV).

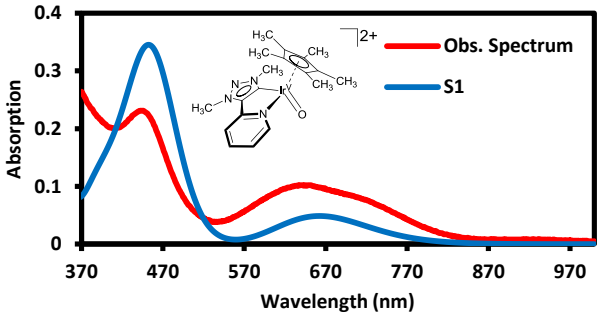

Figure 8: Comparison of observed (red, spectrum obtained 0.5 hr after the 8th addition with initial subtracted) with TD-DFT-derived spectra of proposed intermediate structure **S1** (blue).

Chronological UV/Vis spectra of the first and fourth addition are shown on the left side of Figure 7 while the right side of Figure 7 shows the concurrent pressure and UV/Vis traces at relevant wavelengths. Absorbance at 370 nm captures the shoulder of cerium(IV) absorption and illustrates how quickly cerium(IV) is consumed in the reaction. After the initial addition, the solution absorbs most strongly at 450 nm and 612 nm but quickly decays to the initial spectra.

TD-DFT calculated spectra[70,79] of complex **4c** in an Ir^V=O state predict the pattern of broad and sharp absorption at 670 and 460 nm observed following 8 additions of 20 cerium(IV) equivalents (Figure 8, Calculated spectra of additional conceivable intermediates and in Supporting Information). Notably absent are spectral features consistent with the loss of the Cp* moiety (Figure S5).

Comparing the chronological UV/Vis spectra of the first addition with the fourth suggests the transition from 612 nm to 584 represents a catalytic step prior to the oxygen evolving step, but after the catalyst resting state. Logically, this would represent a transition state similar to the calculated structure **S4** (Ir^{IV}-OH). Indeed, there are strong similarities between the calculated spectra of **S4** and the initial spectra obtained from the 4th through the 8th injections (*cf.* Figure S7, **S4** doublet; Figure 7, Bottom left, traces 0.01-0.34 h). However, the majority of oxygen production occurs during the first hour of reaction, well before many other potentially significant spectral changes and consequently no spectral features were found to directly correlate with the measured rate determining steps of oxygen evolution detailed in Scheme 4.

In contrast to Grotjahn et al.[33] no precipitate was observed at any point. Dynamic light scattering measurements of a 5 mM solution of **4a** in 1N HNO_3 following addition of 20 equivalents of CAN produced variable scattering intensities over time. Scattering indicating sizes as large as 1000 nm were observed by the fourth addition of 20 equivalents; however application of a slight vacuum to the solution causes a decrease in the observed size. Additionally, after 40 hours at atmospheric pressure, particle sizes returned to the baseline measurements of typical cerium(IV)/cerium(III) solutions[71] (*cf.* ibid.; Fig SI-31 and this work; Fig. S12). These two observations strongly suggest that any scattering intensity observed via DLS is derived from the nucleation of dioxygen and not from nanoparticulates or nanoclusters.

In an attempt to further elucidate the reaction mechanism, NMR measurements under identical conditions indicated that **4a** undergoes rapid solvolysis when dissolved in water to produce a

mixture of **4a** and **4c** with a chloride counter ion in a 4:1 ratio. Following addition of 10 equiv. cerium(IV) to the 1 mM NMR sample, integrals of both **4a** and **4c** decrease and the ratio of **4a**:**4c** decreases from 4:1 to 2:1. Repeating the experiment with the addition of 2 equiv cerium(IV) establishes a 3:1 ratio of **4a**:**4c**. The integrals and ratios remained constant over several days, yet all signals disappeared upon addition of a second 10 equiv cerium(IV), indicating the formation of a paramagnetic species. Addition of 20 equiv CAN to a fresh solution of **4a** buffered in 1 N HNO_3 yielded identical results. NMR signals at 8.25 ppm lends support to the formation of formaldehyde which is in agreement with proposed oxidation mechanisms of carbene wingtip methyl groups.[32,72] Although the Cp* methyl signal is noticeably absent from the spectra of **4a** following addition of CAN, broadened signals of the chelating carbene are clearly present.

One explanation that encompasses the DLS, NMR, UV/Vis, and manometric data is fast iridium(III) oxidation to iridium(IV/V) followed by slower, rate limiting oxygen evolution[73] with a potentially concurrent reaction leading to oxidation of the Cp* methyls. However, calculated UV/Vis spectra suggests retention of the Cp* moiety at least up to 160 equivalents of cerium(IV) with 0.5 mM **4a**.

In spite of the sigmoidal oxidation kinetics, which are frequently associated with the formation of a heterogeneous active species, negative results from dynamic light scattering experiments, a lack of carbon dioxide from headspace gases, and significantly faster rate of reaction compared to IrO_2 all reinforce the molecular nature of active species derived from **4a** following a reaction that is dependent on the ligands around the Cp*Ir fragment. While it is difficult, with complete certainty, to eliminate the presence of a heterogeneous species active towards water oxidation, this work shows the most competent catalytically active species under these conditions is likely a molecular species catalysing sequential first-order molecular reactions leading to oxygen evolution. Mesoionic triazolylidenes may be particularly suitable as ligands for the ensuing redox processes, as their strongly mesoionic character is capable of stabilizing various redox states and should assist in proton-coupled electron transfer (PCET) steps. Proton transfer from a putative iridium hydroxide intermediate to the triazolylidene ligand and may thus support the oxidation of the iridium center (Scheme 5). Previous results with related abnormal carbene ligands demonstrated that the mesoionic carbene ligand is involved in hydrogen exchange reactions and in metal-catalyzed E–H bond breaking processes (Scheme 4).[74,75]

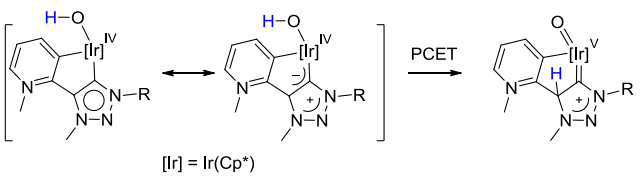

Scheme 5

Conclusions

A variety of iridium complexes comprising mesoionic carbene ligands were synthesized and found to serve as competent precatalysts for the oxidation of water. Turnovers above 30,000 were recorded for the most active catalytic system. This turnover number is limited by the availability of sacrificial oxidant and not by the robustness of the catalyst, which suggests these types of catalysts for continuous water oxidation processes. Mechanistic investigations, especially under stoichiometric or near stoichiometric conditions, strongly support a tunable molecular species. Additionally, dynamic light scattering measurements support the absence of light scattering particles not incipiently present in cerium solutions. While it is not possible to definitively exclude multiple active catalytic species of differing composition, strict adherence to a universal interpretation of the data presented in this work strongly suggests the presence of a homogeneous, tunable, and long-lived iridium water oxidation catalyst with further support from mechanistic studies of similar dinuclear iridium complexes.[76] Future work is directed towards developing an intimate understanding of the catalytic mechanism and exploiting that understanding to increase catalytic activity as well as to incorporate the complexes into a photochemically powered system that does not require the presence of a sacrificial oxidant.

Experimental Section

General

All syntheses of the iridium complexes were carried out under an inert atmosphere of N_2 using Schlenk technique and dry solvents. Purifications, including column chromatography, were performed in air using commercial solvents. All ^{1}H and ^{13}C{^{1}H} NMR spectra were recorded at room temperature on Bruker or Varian spectrometers and chemical shifts were referenced to $SiMe_4$ for organic solvents and to the temperature-corrected residual DHO peak in aqueous experiments (δ in ppm, *J* in Hz). The ligand precursors **L4** and **L6**,[24] the precursor compounds 2-(1-methyl-1*H*-1,2,3-triazol-4-yl)pyridine,[24] 2-(1-phenyl-1*H*-1,2,3-triazol-4-yl)pyridine,[24] 5-methyl-1-phenyl-1*H*-1,2,3-triazole,[77] $[Cp^*IrCl_2]_2$,[78] and the complexes **9** and **10**[28] were prepared according to literature procedures. All other reagents were purchased from commercial sources and were used as received.

L1: A suspension of 2-(1-phenyl-1*H*-1,2,3-triazol-4-yl)pyridine (460 mg, 2.07 mmol) and MeOTf (0.41 mg, 2.48 mmol) in CH_2Cl_2 (5 mL) was stirred at 0° C for 30 minutes. Excess Et_2O was added and the supernatant was removed by decantation. The tan oil was repeatedly washed with Et_2O. NMR spectroscopy of the crude sample indicated non-selective methylation and the presence of two compounds **L1** and **L6** in approximate 2:1 ratio. They were separated by preparative TLC using SiO_2 plates and MeCN/CH_2Cl_2 (1:3 v/v) as eluent. **L6** eluted first;[24] the second band contained **L1** and was extracted from SiO_2 by stirring in MeOH and subsequent filtration. The volatiles were removed under reduced pressure and the residue was dissolved in CH_2Cl_2 and filtered again. The solvent was evaporated and pentane was added. The precipitate was collected and dried in vacuo, thus giving **L1** as a white solid (150 mg, 20%). ^{1}H NMR (CD_3CN, 400 MHz): 9.09 (s, 1H, H_{trz}), 8.79 (d, $^3J_{HH}$ = 6.2 Hz, 1H, H_{py}), 8.58 (t, $^3J_{HH}$ = 8.0 Hz, 1H, H_{py}), 8.51 (d, $^3J_{HH}$ = 8.0 Hz, 1H, H_{py}), 8.0 (dd, $^3J_{HH}$ = 8.0 Hz, $^3J_{HH}$ = 6.2 Hz, 1H, H_{py}), 7.97 (d, $^3J_{HH}$ = 7.4 Hz, 2H, H_{Ph}), 7.68 (d, $^3J_{HH}$ = 7.4 Hz, 2H, H_{Ph}), 7.59 (t, $^3J_{HH}$ = 7.4 Hz, 1H, H_{Ph}), 4.53 (s, 3H, N_{trz}–CH_3). ^{13}C{^{1}H} NMR ($CDCl_3$, 100 MHz): 147.4, 146.3, 145.8, 139.5, 136.5, 130.3, 130.1, 129.2,

127.1, 126.7 (C_{trz}–H), 121.3, 48.6 (N_{trz}–CH_3). Anal. calcd. for $C_{15}H_{13}F_3N_4O_3S$ (386.35): C, 46.63; H, 3.39; N, 14.50 %. Found: C, 46.58; H, 3.31; N, 14.39 %.

L3: The procedure was identical to that described for **L1** starting from 2-(1-methyl-1*H*-1,2,3-triazol-4-yl)pyridine (400 mg, 2.50 mmol) and MeOTf (450 mg, 2.75 mmol), thus giving a crude mixture of **L3** and **L4** in approximate 1:1 ratio. Preparative TLC purification yielded **L3** as the second fraction, which was isolated as described for **L1**, yielding the title product as a white solid (195 mg, 24%). ^{1}H NMR (CD_3CN, 500 MHz): δ 8.74 (d, $^3J_{HH}$ = 6.2 Hz, 1H, H_{py}), 8.58 (s, 1H, H_{trz}), 8.54 (t, $^3J_{HH}$ = 7.8 Hz, 1H, H_{py}), 8.43 (d, $^3J_{HH}$ = 7.8 Hz, 1H, H_{py}), 7.97 (dd, $^3J_{HH}$ = 7.8 Hz, $^3J_{HH}$ = 6.2 Hz, 1H, H_{py}), 4.46 (s, 3H, N_{py}–CH_3), 4.24 (s, 3H, N_{trz}–CH_3). ^{13}C{^{1}H} NMR ($CDCl_3$, 125 MHz): δ 147.0, 145.6, 138.6, 138.4, 129.2 (C_{trz}–H), 128.8, 126.6, 48.4 (N_{py}–CH_3), 37.1 (N_{trz}–CH_3). Anal. calcd. for $C_{10}H_{11}F_3N_4O_3S$ (324.28): C, 37.04; H, 3.42; N, 17.28 %. Found: C, 37.02; H, 3.33; N, 16.97 %.

L5: A mixture of 5-methyl-1-phenyl-1*H*-1,2,3-triazole (200 mg, 1.26 mmol) and 2-bromopyridine (198 mg, 1.26 mmol) was heated in a sealed vial at 160 °C for 36 h. The resulting brown solid was dissolved in H_2O (50 mL) and excess $NaPF_6$ was added. An immediate precipitation was observed. The mixture was stirred for 1 h and then filtered. The residue was washed with copious amounts of H_2O and subsequently with Et_2O and dried in vacuo to give **L5** as a white solid (250 mg, 52%). Recrystallization from MeCN/Et_2O yielded analytically pure material. ^{1}H NMR (CD_3CN, 500 MHz): δ 9.16 (s, 1H, H_{trz}), 8.75 (d, $^3J_{HH}$ = 4.7 Hz, 1H, H_{py}), 8.24 (td, $^3J_{HH}$ = 7.6 Hz, $^4J_{HH}$ = 1.6 Hz, 1H, H_{py}), 8.19 (d, $^3J_{HH}$ = 7.6 Hz, 1H, H_{py}), 7.88–7.77 (m, 6H, H_{py}+H_{Ph}), 2.61 (s, 3H, C_{trz}–CH_3). ^{13}C{^{1}H} NMR (CD_3CN, 125 MHz): δ 149.9, 146.9, 142.8, 141.2, 133.8, 132.8, 130.6, 127.8, 125.76, 125.75, 125.69, 125.67 (C_{trz}–H), 115.2, 9.6 (CH_3). Anal. calcd. for $C_{14}H_{13}F_6N_4P$ (382.24): C, 43.99; H, 3.43; N, 14.66 %. Found: C, 44.00; H, 3.37; N, 14.46 %.

L7: A suspension of 2-(1-phenyl-1*H*-1,2,3-triazol-4-yl)pyridine (370 mg, 1.67 mmol) and MeOTf (1.37 mg, 8.3 mmol) in dry CH_2Cl_2 (8 mL) was stirred at 45 °C for 12 h. The formed precipitate was collected by filtration, washed with CH_2Cl_2 and then with Et_2O and dried in vacuo to afford **L7** as a white solid (606 mg, 66%). ^{1}H NMR (500 MHz, CD_3CN): 9.40 (s, 1H, H_{trz}), 9.10 (d, $^3J_{HH}$ = 6.1 Hz, 1H, H_{py}), 8.79 (td, $^3J_{HH}$ = 7.9 Hz, $^4J_{HH}$ = 0.8 Hz, 1H, H_{py}), 8.39 (dd, $^3J_{HH}$ = 7.9 Hz, $^4J_{HH}$ = 1.3 Hz, 1H, H_{py}), 8.35 (ddd, $^3J_{HH}$ = 7.9 Hz, $^3J_{HH}$ = 6.1 Hz, $^4J_{HH}$ = 1.3 Hz, 1H, H_{py}), 8.01–7.97 (m, 2H, H_{Ph}), 7.81–7.75 (m, 3H, H_{Ph}), 4.37 (s, 3H, N_{trz}–CH_3), 4.36 (s, 3H, N_{py}–CH_3). ^{13}C{^{1}H} NMR (CD_3CN, 125 MHz): δ149.8, 147.3, 136.7, 134.9, 133.6, 132.8, 131.6, 131.4 (C_{trz}–H), 130.8, 122.4, 48.3 (N_{py}–CH_3), 40.2 (N_{trz}–CH_3). Anal. calcd. for $C_{17}H_{16}F_6N_4O_6S_2$ (550.45): C, 37.09; H, 2.93; N, 10.18 %. Found: C, 36.83; H, 2.74; N, 10.48 %.

L8: Compound **L8** was prepared analogously to **L7** starting from 2-(1-methyl-1*H*-1,2,3-triazol-4-yl)pyridine (400 mg, 2.50 mmol) and MeOTf (1.64 g, 10 mmol) and was obtained as a white solid (1.10 g, 90%). ^{1}H NMR (DMSO-d_6, 300 MHz): δ 9.37 (d, $^3J_{HH}$ = 5.8 Hz, 1H, H_{py}), 9.23 (s, 1H, H_{trz}), 8.86 (td, $^3J_{HH}$ = 7.9 Hz, $^4J_{HH}$ = 0.8 Hz, 1H, H_{py}), 8.48–8.42 (m, 2H, H_{py}), 4.46, 4.27 (2 × s, 3H, N_{trz}–CH_3), 4.26 (s, 3H, N_{py}–CH_3). ^{13}C{^{1}H} NMR (CD_3CN, 125 MHz): δ 149.6, 146.9, 17.6, 134.5 (C_{trz}–H), 132.7, 132.1, 130.8, 47.9 (N_{py}–CH_3), 40.9, 39.6 (2 × N_{trz}–CH_3). Anal. calcd. for $C_{12}H_{14}F_6N_4O_6S_2$ (488.38): C, 29.51; H, 2.89; N, 11.47 %. Found: C, 30.22; H, 3.01; N, 11.29 %.

Complexes 1 and 2: A mixture of **L1** (92 mg, 0.25 mmol), AgOAc (63 mg, 0.37 mmol) and $[Cp^*IrCl_2]_2$ (100 mg, 0.13 mmol) in MeOH (10 mL) was refluxed for 24 h and then filtered through Celite. The filtrate was concentrated to ca. 2 mL, which induced crystallization of the orange complex **1** (50 mg, 20%). The mother liquor was evaporated and the residue washed with copious amounts of $CHCl_3$ until the washing was essentially colorless, thus leaving complex **2** as a yellow solid (30 mg, 12%). Analytical data for **1**: ^{1}H NMR (CD_3CN, 400 MHz): δ 9.06 (s, 1H, H_{trz}), 8.71 (d, $^3J_{HH}$ = 7.2 Hz, 1H, H_{py}), 8.31 (d, $^3J_{HH}$ = 6.1 Hz, 1H, H_{py}), 8.03 (d, $^3J_{HH}$ = 7.7 Hz, 2H, H_{Ph}), 7.75–7.66 (m, 3H, H_{Ph}), 7.59 (dd, $^3J_{HH}$ = 7.2 Hz, $^3J_{HH}$ = 6.1 Hz, 1H, H_{py}), 4.46 (s, 3H, N–CH_3), 1.80 (s, 15H, C_{Cp}–CH_3). ^{13}C{^{1}H} NMR (CD_3CN, 100 MHz): δ 162.0 (C_{py}–Ir), 152.0, 150.4, 147.4, 139.2, 136.4 130.8, 130.5, 125.7, 124.8 (C_{trz}–H), 121.3, 90.9 (C_{Cp}), 47.9 (N–CH_3), 8.5 (C_{Cp}–CH_3). Anal. calcd. for $C_{25}H_{27}ClF_3IrN_4O_3S$ (478.24): C, 40.13; H, 3.64; N, 7.49 %. Found: C, 39.59; H, 3.52; N, 7.32 %. Single crystals of **1** that were suitable for X-ray diffraction were obtained from the corresponding tetraphenylborate salt. This salt was obtained by adding $NaBPh_4$ (20.5 mg, 0.06 mmol) to a solution of **1** (10 mg, 0.01 mmol) in MeOH (2 mL). After stirring for 30 minutes, the yellow precipitate was collected, washed twice with MeOH and finally with Et_2O and then dried in vacuo. The ^{1}H NMR spectrum does not show any significant change except for the new resonances at δ 7.30, 7.01 and 6.86 due to the BPh_4^- anion. The ^{19}F NMR spectrum is empty and does not show any signal in the range expected for the triflate anion.

Analytical data for **2**: ^{1}H NMR (CD_3CN, 500 MHz): δ 9.17 (s, 1H, H_{trz}), 8.79 (d, $^3J_{HH}$ = 6.1 Hz, 1H, H_{py}), 8.62 (t, $^3J_{HH}$ = 8.0 Hz, 1H, H_{py}), 8.50 (dd, $^3J_{HH}$ = 8.0 Hz, $^4J_{HH}$ = 1.4 Hz, 1H, H_{py}), 8.05 (ddd, $^3J_{HH}$ = 8.0 Hz, $^3J_{HH}$ = 6.2 Hz, $^4J_{HH}$ = 1.4 Hz, 1H, H_{py}), 7.90, 7.79 (2 × dd, $^3J_{HH}$ = 7.4 Hz, $^4J_{HH}$ = 1.3 Hz, 1H, H_{Ph}), 7.32 7.25 (2 × td, $^3J_{HH}$ = 7.4 Hz, $^4J_{HH}$ = 1.3 Hz, 1H, H_{Ph}), 4.56 (s, 3H, N–CH_3), 1.82 (s, 15H, C_{Cp}–CH_3). ^{13}C{^{1}H} NMR (CD_3CN, 125 MHz): δ 148.8 (C_{Ph}–Ir), 147.6, 145.9, 140.0, 139.5, 137.2, 133.9, 129.5, 129.3, 127.4, 124.1 (C_{trz}–H), 123.5, 113.7, 90.4 (C_{Cp}), 48.8 (N–CH_3), 8.4 (C_{Cp}–CH_3). Anal. calcd. for $C_{25}H_{27}ClF_3IrN_4O_3S$ (478.24): C, 40.13; H, 3.64; N, 7.49 %.

Complex 3: Compound **L3** (120 mg, 0.37 mmol), AgOAc (124 mg, 0.74 mmol) and $[Cp^*IrCl_2]_2$ (147 mg, 0.18 mmol) was refluxed in dry MeOH (12 mL) for 18 h. The reaction mixture was filtered through Celite and concentrated to ca. 4 mL. Crystallization was induced upon standing at room temperature and afforded pure **3** as an orange solid (60 mg, 35%). ^{1}H NMR (CD_3CN, 300 MHz): δ 8.65 (dd, $^3J_{HH}$ = 7.7 Hz, $^4J_{HH}$ = 0.7 Hz, 1H, H_{py}), 8.52 (s, H_{trz}, 1H), 8.24 (dd, $^3J_{HH}$ = 5.9 Hz, $^4J_{HH}$ = 0.7 Hz, 1H, H_{py}), 7.53 (dd, $^3J_{HH}$ = 7.7 Hz, $^3J_{HH}$ = 5.9 Hz, 1H, H_{py}), 4.33 (s, 3H, N_{py}–CH_3), 4.29 (s, 3H, N_{trz}–CH_3), 1.74 (s, 15H, C_{Cp}–CH_3). ^{13}C{^{1}H} NMR (CD_3CN, 125 MHz): δ 161.5 (C_{py}–Ir), 151.6, 150.6, 146.2, 138.5, 127.62 (C_{trz}–H), 125.1, 90.3 (C_{Cp}), 47.4 (N_{py}–CH_3), 38.6 (N_{trz}–CH_3), 8.1 (C_{Cp}–CH_3). Anal. calcd. for $C_{20}H_{25}ClF_3IrN_4O_3S$ (686.17): C, 35.01; H, 3.67; N, 8.17 %. Found: C, 34.88; H, 3.49; N, 7.99 %.

Complex 4a: A suspension of **L4** (70 mg, 0.216 mmol), Ag_2O (50 mg, 0.216 mmol) and $[Cp^*IrCl_2]_2$ (86 mg, 0.108 mmol) in

CH_2Cl_2 (15 mL) was stirred for 18 h. After filtration through Celite, the volume was reduced to ca. 1 mL and excess Et_2O was added. The resulting precipitate was filtered off and purified by column chromatography (SiO_2; CH_2Cl_2/MeCN). The yellow fraction was collected, evaporated, and dried in vacuo to give complex **4a** as a yellow solid (80 mg, 54%). ^{1}H NMR (CD_3CN, 300 MHz): δ 8.74 (d, $^3J_{HH}$ = 5.7 Hz, 1H, H_{py}), 8.10–8.02 (m, 2H, H_{py}), 7.49–7.41 (m, 1H, H_{py}), 4.51, 4.30 (2 × s, 3H, N_{trz}–CH_3), 1.73 (s, 15H, C_{Cp}–CH_3). ^{13}C{^{1}H} NMR (CD_3CN, 125 MHz): δ 157.5 (C_{trz}–Ir), 153.9, 148.9, 147.9, 139.9, 126.4, 121.4, 91.1 (C_{Cp}), 39.9, 38.9 (2 × N_{trz}–CH_3), 8.8 (C_{Cp}–*C*H_3). Anal. calcd. for $C_{20}H_{25}ClF_3IrN_4O_3S$ (686.17): C, 35.01; H, 3.67; N, 8.17 %. Found: C, 34.98; H, 3.68; N, 8.06 %.

Complex 4b: A mixture of **4a** (100 mg, 0.15 mmol) and AgOTf (56 mg, 0.218 mmol) was refluxed in MeCN (10 mL) for 24 h. It was filtered through Celite and the filtrate was evaporated to dryness, washed with $CHCl_3$ (4 × 1 mL), and dried in vacuo, thus affording complex **4b** as a yellowish solid (78 mg, 78%). ^{1}H NMR (CD_3CN, 300 MHz): δ 9.20 (d, $^3J_{HH}$ = 5.6 Hz, 1H, H_{py}), 8.27–8.14 (m, 2H, H_{py}), 7.69 (ddd, $^3J_{HH}$ = 7.4 Hz, $^3J_{HH}$ = 5.6 Hz, $^4J_{HH}$ = 2.0 Hz, H_{py}, 1H), 4.59, 4.53 (2 × s, 3H, N_{trz}–CH_3), 1.70 (s, 15H, C_{Cp}–CH_3). ^{13}C{^{1}H} NMR (CD_3CN, 125 MHz): δ 154.6 (C_{trz}–Ir), 151.1, 149.4, 149.3, 141.5, 127.3, 122.3, 93.7 (C_{Cp}), 40.5, 39.1 (2 × N_{trz}–CH_3), 8.7 (C_{Cp}–*C*H_3). Anal. calcd. for $C_{23}H_{28}F_6IrN_5O_6S_2$ (840.84): C, 32.85; H, 3.36; N, 8.33 %. Found: C, 32.88; H, 3.15; N, 8.33 %.

Complex 4c: Complex **4a** (60 mg, 0.087 mmol), AgOTf (45 mg, 0.17 mmol) and a drop of water (20 μL, 1.2 mmol) in CH_2Cl_2 (10 mL) was sonicated during 10 min. at 40 ºC and subsequently stirred for 16 h at room temperature,. The crude mixture was filtered through Celite. Slow evaporation of the filtrate afforded pale yellow crystals that were washed with Et_2O (62 mg, 87%). ^{1}H NMR (500 MHz, D_2O) δ 9.14 (d, 1H, $^3J_{HH}$ = 5.5 Hz, H_{py}), 8.31 (t, 1H, $^3J_{HH}$ = 8.0 Hz, H_{py}), 8.22 (d, 1H, $^3J_{HH}$ = 8.0 Hz, H_{py}), 7.76 (t, 1H, $^3J_{HH}$ = 6.6 Hz, H_{py}), 4.59 (s, 3H, $N_{trz}CH_3$), 4.52 (s, 3H, N_{trz}Me) 1.80 (s, C_{Cp}–CH_3, 15H). ^{13}C{^{1}H}NMR (125 MHz, $CDCl_3$) **δ** 155.2 (C_{trz}–Ir), 153.6 (CH_{py}) 150.0 (C_{qtrz}), 149.0 (C_{qpy}), 141.4 (CH_{py}), 127.2 (CH_{py}), 121.7 (CH_{py}), 90.6 (C_{Cp}), 40.3 (NCH_3), 38.5 (NCH_3), 8.5 (5 Me). Anal. calcd. for $C_{21}H_{27}F_6IrN_4O_7S_2$: C, 30.88; H, 3.04; N, 6.55. Found: C, 30.84; H, 3.33; N, 6.85.

Complex 5: A mixture of **L5** (100 mg, 0.26 mmol), Ag_2O (61 mg, 0.26 mmol), and $[Cp^*IrCl_2]_2$ (104 mg, 0.13 mmol) in CH_2Cl_2 (12 mL) was stirred at room temperature for 24 h. After filtration through Celite, the volume of the filtrate was reduced to ca. 1 mL and excess Et_2O was added. The formed precipitate was isolated and dried, giving **5** as an orange solid (82 mg, 31%). ^{1}H NMR (CD_3CN, 500 MHz): δ 8.85 (dt, $^3J_{HH}$ = 5.7 Hz, $^4J_{HH}$ = 1.0, Hz, 1H, H_{py}), 8.31–8.29 (m, 2H, H_{py}), 7.82–7.73 (m, 6H, H_{py}+H_{Ph}), 2.67 (s, 3H, C_{trz}–CH_3), 1.83 (s, C_{Cp}–CH_3, 15H). ^{13}C{^{1}H} NMR ($CDCl_3$, 125 MHz): δ 152.7 (C_{trz}–Ir), 151.9, 150.5, 142.9, 142.6, 134.7, 132.2, 130.4, 127.9, 125.8, 114.7, 91.8 (C_{Cp}), 30.0 (C_{trz}–*C*H_3), 8.9 (C_{Cp}–*C*H_3). Anal. calcd. for $C_{24}H_{27}ClF_6IrN_4P$ (744.13): C, 38.74; H, 3.66; N, 7.53 %. Found: C, 38.59; H, 3.52; N, 7.48 %.

Complex 6a: Compound **L6** (88 mg, 0.24 mmol), Ag_2O (55 mg, 0.24 mmol), and $[Cp^*IrCl_2]_2$ (95 mg, 0.12 mmol) were suspended in CH_2Cl_2 (15 mL) and stirred for 18 h. The mixture was filtered through Celite and concentrate to ca. 1 mL. Addition of excess Et_2O resulted in the precipitation of yellow solid, which was isolated and purified by flash chromatography using SiO_2 and CH_2Cl_2/MeCN (1:4 v/v), yielded **6a** as a yellow solid (110 mg, 61%). ^{1}H NMR ($CDCl_3$, 300 MHz): δ 8.76 (d, $^3J_{HH}$ = 5.8 Hz, 1H, H_{py}), 8.20 (d, $^3J_{HH}$ = 7.8 Hz, 1H, H_{py}), 8.08 (td, $^3J_{HH}$ = 7.8 Hz, $^4J_{HH}$ = 1.4 Hz, 1H, H_{py}), 8.06–8.0 (m, 2H, H_{Ph}), 7.66–7.58 (m, 3H, H_{Ph}), 7.44 (ddd, $^3J_{HH}$ = 7.8 Hz, $^3J_{HH}$ = 5.8 Hz, $^4J_{HH}$ = 1.4 Hz, 1H, H_{py}), 4.71 (s, 3H, N_{trz}–CH_3), 1.47 (s, 15H, C_{Cp}–CH_3). ^{13}C{^{1}H} NMR ($CDCl_3$, 125 MHz): δ 155.9 (C_{trz}–Ir), 153.1, 149.3, 148.7, 140.1, 138.1, 130.9, 129.8, 125.8, 125.6, 121.9, 91.1 (C_{Cp}), 39.5 (N_{trz}–CH_3), 8.9 (C_{Cp}–*C*H_3). Anal. calcd. for $C_{25}H_{27}ClF_3IrN_4O_3S$ (748.24): C, 40.13; H, 3.64; N, 7.49 %. Found: C, 39.98; H, 3.60; N, 7.25 %.

Complex 6b: Complex **6a** (100 mg, 0.134 mmol) was refluxed with AgOTf (52 mg, 0.20 mmol) in MeCN (10 mL) for 24 h. The mixture was filtered through Celite and all volatiles were removed. The residue was washed with $CHCl_3$ (4 × 1 mL) and dried in vacuo, thus affording **6b** as a pale yellow solid (85 mg, 70%). ^{1}H NMR (CD_3CN, 300 MHz): δ 8.95 (d, $^3J_{HH}$ = 5.8 Hz, 1H, H_{py}), 8.30 (t, $^3J_{HH}$ = 7.8 Hz, 1H, H_{py}), 8.20 (d, $^3J_{HH}$ = 7.8 Hz, 1H, H_{py}), 7.79 (m, 5H, H_{Ph}), 7.73 (dd, $^3J_{HH}$ = 7.8 Hz, $^3J_{HH}$ = 5.8 Hz, 1H, H_{py}), 4.60 (s, 3H, N_{trz}–CH_3), 1.47 (s, 15H, C_{Cp}–CH_3). ^{13}C{^{1}H} NMR (CD_3CN, 125 MHz): δ 155.1 (C_{trz}–Ir), 150.1, 149.9, 149.1, 141.6, 137.6, 131.8, 130.6, 127.6, 125.4, 122.4, 93.8 (C_{Cp}), 39.5 (N_{trz}–CH_3), 8.3 (C_{Cp}–*C*H_3). Anal. calcd. for $C_{28}H_{30}F_6IrN_5O_6S_2$ (902.91): C, 37.25; H, 3.35; N, 7.76 %. Found: C, 37.23; H, 3.22; N, 7.74 %.

Complex 7: A suspension of **L7** (200 mg, 0.364 mmol), Ag_2O (84 mg, 0.36 mmol), and $[Cp^*IrCl_2]_2$ (144 mg, 0.18 mmol) in MeCN (25 mL) was refluxed for 24 h. The mixture was filtered through Celite under an N_2 atmosphere and the volatiles were removed. The residue was dissolved in CH_2Cl_2 and filtered again through Celite, concentrated to ca. 1 mL and treated with excess Et_2O. The formed precipitate was collected and dried in vacuo, yielding **7** a yellow solid (120 mg, 33%). ^{1}H NMR (CD_3CN, 600 MHz): δ 9.18 (d, $^3J_{HH}$ = 6.2 Hz, 1H, H_{py}), 8.83 (t, $^3J_{HH}$ = 7.9, 1H, H_{py}), 8.49 (dd, $^3J_{HH}$ = 7.9 Hz, $^4J_{HH}$ = 1.3 Hz, 1H, H_{py}), 8.35 (ddd, $^3J_{HH}$ = 7.9 Hz, $^3J_{HH}$ = 6.2 Hz, $^4J_{HH}$ = 1.3 Hz, 1H, H_{py}), 7.85 (dd, $^3J_{HH}$ = 7.6 Hz, $^4J_{HH}$ = 1.4 Hz, 1H, H_{Ph}), 7.81 (d, $^3J_{HH}$ = 7.6 Hz, $^4J_{HH}$ = 1.4 Hz, 1H, H_{Ph}), 7.35, 7.30 (2 × td, $^3J_{HH}$ = 7.6 Hz, $^4J_{HH}$ = 1.4 Hz, 12H, H_{Ph}), 4.34 (s, 3H, N_{py}–CH_3), 4.19 (s, 3H, N_{trz}–CH_3), 1.57 (s, 15H, C_{Cp}–CH_3). ^{13}C{^{1}H} NMR ($CDCl_3$, 125 MHz): δ 149.4, 147.6, 146.6 (C_{trz}–Ir), 144.1(C_{Ph}–Ir), 141.8, 138.0, 137.3, 135.5, 133.4, 130.3, 130.1, 124.8, 114.4, 93.4 (C_{Cp}), 47.9 (N_{py}–CH_3), 38.6 (N_{trz}–CH_3), 8.4 (C_{Cp}–*C*H_3). Anal. calcd. for $C_{29}H_{32}F_6IrN_5O_6S_2$ (916.93): C, 37.99; H, 3.52; N, 7.64 %. Found: C, 37.57; H, 3.50; N, 7.42 %.

Complex 8: A suspension containing **L8** (86 mg, 0.18 mmol), Ag_2O (41 mg, 0.18 mmol), and $[Cp^*IrCl_2]_2$ (71 mg, 0.09 mmol) in MeCN (10 mL) was refluxed for 24 h. The mixture was filtered through Celite and the filtrate was concentrated to ca. 1 mL. Excess Et_2O was added and the formed precipitate was collected and dried, yielding **8** as a yellow solid (72 mg, 40%). ^{1}H NMR (CD_3CN, 500 MHz): δ 8.71 (d, $^3J_{HH}$ = 7.6 Hz, 1H, H_{py}), 8.30 (d, $^3J_{HH}$ = 6.1 Hz, 1H, H_{py}), 7.51 (dd, $^3J_{HH}$ = 7.6 Hz, $^3J_{HH}$ = 6.1 Hz, 1H, H_{py}), 4.61 (s, 3H, N_{trz}–CH_3), 4.59 (s, 3H, N_{py}–CH_3), 4.32 (s, 3H, N_{trz}–CH_3), 1.84 (s, 15H, C_{Cp}–CH_3). ^{13}C{^{1}H} NMR

(CD_3CN, 100 MHz): δ 154.6 (C_{trz}–Ir), 154.0 (C_{py}–Ir), 152.9, 152.6, 148.7, 139.9, 125.2, 110.2 (N*C*CH_3), 94.6 (C_{Cp}), 49.6 (N_{trz}–CH_3), 43.8 (N_{py}–CH_3), 39.9 (N_{trz}–CH_3), 8.8 (C_{Cp}–CH_3), 4.6 (NCCH_3). Anal. calcd. for $C_{24}H_{30}F_6IrN_5O_6S_2$ (854.86): C, 33.72; H, 3.54; N, 8.19 %. Found: C, 33.59; H, 3.52; N, 7.92 %.

Dynamic Oxygen Evolution Measurement: Complexes were investigated for water oxidation by mixing them with ceric ammonium nitrate (CAN) in water buffered with 1N nitric acid with pressure monitoring and GC analysis as previously described.[20] Extended reactivity experiments were conducted in 20/40/60 mL EPA vials as well as sealed cuvettes enabling concurrent UV/vis spectroscopy.

Time-dependent DFT (TD-DFT). Time dependent calculations were performed at the optimized ground-state geometry via Gaussian 03 software. The unrestricted B3LYP functional was used and the LANL2DZ basis set was applied to all atoms since that basis set has previously resulted in superior agreement of TD-DFT spectra with experimental data[79]. The energy, oscillator strength, and rotatory strength were computed for each of the 70 lowest singlet excitations.[70,80] Electronic transitions were expanded as Gaussian curves with a FWHM (full width at half-maximum) for each peak set to 2.41 eV (3000 cm^{-1}).

Crystal structure determinations. Crystal data were collected using an Oxford Diffraction SuperNova A diffractometer fitted with an Atlas detector. Crystals were measured with monochromated Mo-K_α radiation (0.71073 Å). A twice redundant dataset was collected, assuming that the Friedel pairs are not equivalent. An analytical absorption correction based on the shape of the crystal was performed.[81] The structures were solved by direct methods using SHELXS-97 and refined by full matrix least-squares on F^2 for all data using SHELXL-97.[82] Hydrogen atoms were added at calculated positions and refined using a riding model. Their isotropic temperature factors were fixed to 1.2 times (1.5 times for methyl groups) the equivalent isotropic displacement parameters of the carbon atom the H-atom is attached to. Anisotropic thermal displacement parameters were used for all non-hydrogen atoms. Further crystallographic details are compiled in the Supporting Information. CCDC 850692–850700 contain the supplementary crystallographic data for this paper. These data can be obtained free of charge from the Cambridge Crystallographic Data Centre via www.ccdc.cam.ac.uk/data_request/cif.

Acknowledgements: We thank Yann Ortin and Alexander Gorelov for technical assistance. This work was financially supported by the European Research Council (ERC 208561) and Science Foundation Ireland (SFI), in parts under the Solar Energy Conversion Strategic Research Cluster (grant 07/06/B1160). S.B. gratefully acknowledges support by the National Science Foundation (CHE-1055547).

Notes and references

1 *EIA - 2012 International Energy Outlook*, 2012.
2 J. T. Kiehl and K. E. Trenberth, *Bulletin of the American Meteorological Society*, 1997, **78**, 197–208.
3 N. D. McDaniel and S. Bernhard, *Dalton Trans.*, 2010, **39**, 10021–10030.
4 J. E. Miller, M. D. Allendorf, R. B. Diver, L. R. Evans, N. P. Siegel, and J. N. Stuecker, *J. Mater. Sci.*, 2008, **43**, 4714–4728.
5 R. Brimblecombe, G. F. Swiegers, G. C. Dismukes, and L. Spiccia, *Angew. Chem., Int. Ed.*, 2008, **47**, 7335–7338.
6 G. Seshadri, C. Lin, and A. B. Bocarsly, *J. Electroanal. Chem.*, 1994, **372**, 145–150.
7 A. C. Brooks, K. Basore, and S. Bernhard, *Inorg. Chem.*, 2013, **52**, 5794–800.
8 E. D. Cline, S. E. Adamson, and S. Bernhard, *Inorg. Chem.*, 2008, **47**, 10378–10388.
9 S. W. Gersten, G. J. Samuels, and T. J. Meyer, *J. Am. Chem. Soc.*, 1982, **104**, 4029–4030.
10 J. A. Gilbert, D. S. Eggleston, W. R. Murphy, D. A. Geselowitz, S. W. Gersten, D. J. Hodgson, and T. J. Meyer, *J. Am. Chem. Soc.*, 1985, **107**, 3855–3864.
11 C. Sens, I. Romero, M. Rodríguez, A. Llobet, T. Parella, and J. Benet-Buchholz, *J. Am. Chem. Soc.*, 2004, **126**, 7798–9.
12 R. Zong and R. P. Thummel, *J. Am. Chem. Soc.*, 2005, **127**, 12802–3.
13 Y. V Geletii, B. Botar, P. Kögerler, D. A. Hillesheim, D. G. Musaev, and C. L. Hill, *Angew. Chem., Int. Ed.*, 2008, **47**, 3896–9.
14 A. Sartorel, M. Carraro, G. Scorrano, R. De Zorzi, S. Geremia, N. D. McDaniel, S. Bernhard, and M. Bonchio, *J. Am. Chem. Soc.*, 2008, **130**, 5006–5007.
15 A. Sartorel, P. Miró, E. Salvadori, S. Romain, M. Carraro, G. Scorrano, M. Di Valentin, A. Llobet, C. Bo, and M. Bonchio, *J. Am. Chem. Soc.*, 2009, **131**, 16051–16053.
16 Q. Yin, J. M. Tan, C. Besson, Y. V Geletii, D. G. Musaev, A. E. Kuznetsov, Z. Luo, K. I. Hardcastle, and C. L. Hill, *Science*, 2010, **328**, 342–5.
17 N. S. McCool, D. M. Robinson, J. E. Sheats, and G. C. Dismukes, *J. Am. Chem. Soc.*, 2011, **133**, 11446–11449.
18 J. Limburg, J. S. Vrettos, H. Chen, J. C. de Paula, R. H. Crabtree, and G. W. Brudvig, *J. Am. Chem. Soc.*, 2001, **123**, 423–430.
19 H.-W. Tseng, R. Zong, J. T. Muckerman, and R. Thummel, *Inorg. Chem.*, 2008, **47**, 11763–73.
20 N. D. McDaniel, F. J. Coughlin, L. L. Tinker, and S. Bernhard, *J. Am. Chem. Soc.*, 2008, **130**, 210–217.
21 J. J. Concepcion, J. W. Jurss, J. L. Templeton, and T. J. Meyer, *J. Am. Chem. Soc.*, 2008, **130**, 16462–16463.
22 S. W. Kohl, L. Weiner, L. Schwartsburd, L. Konstantinovski, L. J. W. Shimon, Y. Ben-David, M. A. Iron, and D. Milstein, *Science*, 2009, **324**, 74–77.
23 W. C. Ellis, N. D. McDaniel, S. Bernhard, and T. J. Collins, *J. Am. Chem. Soc.*, 2010, **132**, 10990–10991.
24 L. Bernet, R. Lalrempuia, W. Ghattas, H. Mueller-Bunz, L. Vigara, A. Llobet, and M. Albrecht, *Chem. Commun.*, 2011, **47**, 8058–8060.
25 A. Savini, G. Bellachioma, S. Bolaño, L. Rocchigiani, C. Zuccaccia, D. Zuccaccia, and A. Macchioni, *ChemSusChem*, 2012, **5**, 1415–1419.
26 L. Duan, F. Bozoglian, S. Mandal, B. Stewart, T. Privalov, A. Llobet, and L. Sun, *Nat. Chem.*, 2012, **4**, 418–23.
27 J. F. Hull, D. Balcells, J. D. Blakemore, C. D. Incarvito, O. Eisenstein, G. W. Brudvig, and R. H. Crabtree, *J. Am. Chem. Soc.*, 2009, **131**, 8730–8731.
28 R. Lalrempuia, N. D. McDaniel, H. Müller-Bunz, S. Bernhard, and M. Albrecht, *Angew. Chem., Int. Ed.*, 2010, **49**, 9765–9768.
29 J. D. Blakemore, N. D. Schley, D. Balcells, J. F. Hull, G. W. Olack, C. D. Incarvito, O. Eisenstein, G. W. Brudvig, and R. H. Crabtree, *J. Am. Chem. Soc.*, 2010, **132**, 16017–16029.
30 A. Savini, G. Bellachioma, G. Ciancaleoni, C. Zuccaccia, D. Zuccaccia, and A. Macchioni, *Chem. Commun.*, 2010, **46**, 9218–9219.
31 D. G. H. Hetterscheid and J. N. H. Reek, *Chem. Commun.*, 2011, **47**, 2712–2714.
32 A. Savini, P. Belanzoni, G. Bellachioma, C. Zuccaccia, D. Zuccaccia, and A. Macchioni, *Green Chem.*, 2011, **13**, 3360–3374.
33 D. B. Grotjahn, D. B. Brown, J. K. Martin, D. C. Marelius, M.-C. Abadjian, H. N. Tran, G. Kalyuzhny, K. S. Vecchio, Z. G. Specht, S. A. Cortes-Llamas, V. Miranda-Soto, C. van Niekerk, C. E. Moore, and A. L. Rheingold, *J. Am. Chem. Soc.*, 2011, **133**, 19024–19027.

34 D. Hong, M. Murakami, Y. Yamada, and S. Fukuzumi, *Energy Environ. Sci.*, 2012, **5**, 5708–5716.
35 H. Junge, N. Marquet, A. Kammer, S. Denurra, M. Bauer, S. Wohlrab, F. Gärtner, M.-M. Pohl, A. Spannenberg, S. Gladiali, and M. Beller, *Chem. Eur. J.*, 2012, **18**, 12749–12758.
36 N. D. Schley, J. D. Blakemore, N. K. Subbaiyan, C. D. Incarvito, F. D'Souza, R. H. Crabtree, and G. W. Brudvig, *J. Am. Chem. Soc.*, 2011, **133**, 10473–10481.
37 K. E. DeKrafft, C. Wang, Z. Xie, X. Su, B. J. Hinds, and W. Lin, *ACS Appl. Mater. Interfaces*, 2012, **4**, 608–613.
38 W. J. Youngblood, S.-H. A. Lee, K. Maeda, and T. E. Mallouk, *Acc. Chem. Res.*, 2009, **42**, 1966–73.
39 C. Herrero, A. Quaranta, W. Leibl, A. W. Rutherford, and A. Aukauloo, *Energy Environ. Sci.*, 2011, **4**, 2353.
40 G. F. Moore, J. D. Blakemore, R. L. Milot, J. F. Hull, H. Song, L. Cai, C. A. Schmuttenmaer, R. H. Crabtree, and G. W. Brudvig, *Energy Environ. Sci.*, 2011, **4**, 2389.
41 S. Y. Reece, J. A. Hamel, K. Sung, T. D. Jarvi, A. J. Esswein, J. J. H. Pijpers, and D. G. Nocera, *Science*, 2011, **334**, 645–8.
42 H. G. Raubenheimer and S. Cronje, *Dalton Trans.*, 2008, 1265–72.
43 P. Mathew, A. Neels, and M. Albrecht, *J. Am. Chem. Soc.*, 2008, **130**, 13534–5.
44 G. Guisado-Barrios, J. Bouffard, B. Donnadieu, and G. Bertrand, *Angew. Chem., Int. Ed.*, 2010, **49**, 4759–62.
45 A. Poulain, D. Canseco-Gonzalez, R. Hynes-Roche, H. Müller-Bunz, O. Schuster, H. Stoeckli-Evans, A. Neels, and M. Albrecht, *Organometallics*, 2011, **30**, 1021–1029.
46 R. Saravanakumar, V. Ramkumar, and S. Sankararaman, *Organometallics*, 2011, **30**, 1689–1694.
47 M. Albrecht, *Chem. Rev.*, 2010, **110**, 576–623.
48 Y. Tulchinsky, M. A. Iron, M. Botoshansky, and M. Gandelman, *Nat. Chem.*, 2011, **3**, 525–31.
49 A. R. Chianese, A. Kovacevic, B. M. Zeglis, J. W. Faller, and R. H. Crabtree, *Organometallics*, 2004, **23**, 2461–2468.
50 M. Heckenroth, E. Kluser, A. Neels, and M. Albrecht, *Angew. Chem., Int. Ed.*, 2007, **46**, 6293–6.
51 G. Ung and G. Bertrand, *Chem. Eur. J.*, 2011, **17**, 8269–72.
52 S. Araki, Y. Wanibe, F. Uno, A. Morikawa, K. Yamamoto, K. Chiba, and Y. Butsugan, *Chem. Ber.*, 1993, **126**, 1149–1155.
53 M. Albrecht, *Chem. Commun.*, 2008, 3601–3610.
54 O. Schuster, L. Yang, H. G. Raubenheimer, and M. Albrecht, *Chem. Rev.*, 2009, **109**, 3445–78.
55 M. Melaimi, M. Soleilhavoup, and G. Bertrand, *Angew. Chem., Int. Ed.*, 2010, **49**, 8810–8849.
56 Complex **11** was isolated as a minor fraction from column purification of complex **4a** by changing the mobile phase after elution of **4a** from CH_2Cl_2/MeCN to pure MeOH. ^{1}H NMR data for **11** (CD_3CN, 300 MHz): δ 8.71 (d, $^3J_{HH}$ = 4.2 Hz, 1H, H_{py}), 7.95–7.83 (m, 3H, H_{py}), 7.79 (t, $^3J_{HH}$ = 7.8 Hz, 1H, H_{py}), 7.65–7.58 (m, 1H, H_{py}), 6.91–6.78 (m, 2H, H_{py}), 4.37, 4.23, 4.05, 3.55 (4 × s, 3H, N_{trz}–CH3), 1.80 (s, 15H, C_{Cp}–CH3).
57 M. Poyatos, J. A. Mata, and E. Peris, *Chem. Rev.*, 2009, **109**, 3677–707.
58 R. A. Binstead and T. J. Meyer, *J. Am. Chem. Soc.*, 1987, **109**, 3287–3297.
59 P. Yu and T. J. O'Keefe, *Journal of The Electrochemical Society*, 2006, **153**, C80.
60 A. Ikeda-Ohno, S. Tsushima, C. Hennig, T. Yaita, and G. Bernhard, *Dalton Trans.*, 2012, **41**, 7190–2.
61 U. Hintermair, S. M. Hashmi, M. Elimelech, and R. H. Crabtree, *J. Am. Chem. Soc.*, 2012, **134**, 9785–9795.
62 A. Petronilho, M. Rahman, J. A. Woods, H. Al-Sayyed, H. Müller-Bunz, J. M. Don MacElroy, S. Bernhard, and M. Albrecht, *Dalton Trans.*, 2012, **41**, 13074–13080.
63 S. M. Barnett, K. I. Goldberg, and J. M. Mayer, *Nat. Chem.*, 2012, **4**, 498–502.
64 R. H. Crabtree, *Chem. Rev.*, 2012, **112**, 1536–1554.
65 D. J. Wasylenko, C. Ganesamoorthy, M. A. Henderson, and C. P. Berlinguette, *Inorg. Chem.*, 2011, **50**, 3662–72.
66 J. Kragten and L. G. Decnop-Weever, *Talanta*, 1978, **25**, 147–150.
67 J. D. Blakemore, N. D. Schley, G. W. Olack, C. D. Incarvito, G. W. Brudvig, and R. H. Crabtree, *Chem. Sci.*, 2011, **2**, 94.
68 S. E. Castillo-Blum, D. T. Richens, and A. G. Sykes, *Inorg. Chem.*, 1989, **28**, 954–960.
69 D. G. Blackmond, *Angew. Chem., Int. Ed.*, 2005, **44**, 4302–20.
70 N. M. O'Boyle, A. L. Tenderholt, and K. M. Langner, *J. Comput. Chem.*, 2008, **29**, 839–45.
71 Z. Codolà, J. M S Cardoso, B. Royo, M. Costas, and J. Lloret-Fillol, *Chem. Eur. J.*, 2013, **19**, 7203–13.
72 C. Zuccaccia, G. Bellachioma, S. Bolaño, L. Rocchigiani, A. Savini, and A. Macchioni, *Inorg. Chem.*, 2012, **2012**, 1462–1468.
73 T. P. Brewster, J. D. Blakemore, N. D. Schley, C. D. Incarvito, N. Hazari, G. W. Brudvig, and R. H. Crabtree, *Organometallics*, 2011, **30**, 965–973.
74 A. Krüger and M. Albrecht, *Aust. J. Chem.*, 2011, **64**, 1113.
75 L. Hammarström and S. Styring, *Energy Environ. Sci.*, 2011, **4**, 2379.
76 A. Petronilho, J. A. Woods, S. Bernhard, M. Albrecht, *Eur. J. Inorg. Chem.*, 2013, DOI: 10.1002/ejic.201300843
77 P. Ykman, G. L'abbé, and G. Smets, *Tetrahedron*, 1971, **27**, 845–849.
78 R. G. Ball, W. A. G. Graham, D. M. Heinekey, J. K. Hoyano, A. D. McMaster, B. M. Mattson, and S. T. Michel, *Inorg. Chem.*, 1990, **29**, 2023–2025.
79 F. J. Coughlin, M. S. Westrol, K. D. Oyler, N. Byrne, C. Kraml, E. Zysman-Colman, M. S. Lowry, and S. Bernhard, *Inorg. Chem.*, 2008, **47**, 2039–2048.
80 N. M. O'Boyle, 2006.
81 Program CrysalisPro Version 1.171.33.55, Oxford Diffraction Limited, 2010.
82 G. M. Sheldrick, *Acta Crystallogr., Sect. A: Found. Crystallogr.*, 2008, **64**, 112–22.